Pergamon

Cement and Concrete Research 30 (2000) 25–35

CEMENT AND CONCRETE RESEARCH

A new image analysis technique for the quantitative assessment of microcracks in cement-based materials

A. Ammouche[a,b,c], D. Breysse[b], H. Hornain[a], O. Didry[d], J. Marchand[c,*]

[a]*Laboratoire d'Etudes et de Recherches sur les Matériaux (LERM) 23, Rue de la Madeleine BP 136, 13631 Arles, France*
[b]*Centre de Développement des Géosciences Appliquées Université de Bordeaux I, 33405 Talence, France*
[c]*CRIB-Department of Civil Engineering Laval University, Quebec G1K 7P4, Canada*
[d]*Electricité de France, Direction des Etudes et Recherches, 77250 Moret Sur Loing, France*

Received 2 February 1999; accepted 30 August 1999

Abstract

The development of a new image analysis technique for the automatic detection and quantification of microcracking in cement-based materials is described. An impregnation technique is used to highlight microcracks and other microdefects (porosity, air bubbles) present in the concrete matrix. Microcrack observations of the polished samples are carried out using an optical microscope. The first step of the image analysis process consists of extracting the various defects from the observed image. The extraction process is essentially an automated thresholding operation carried out on the grey-level histogram. The second step consists of automatically sorting the various extracted defects on the basis of a certain number of shape factors. For the third step, an innovative technique is used to reconnect several neighboring microscopic fields. Finally, the characteristics of the cracking pattern are quantitatively determined using classical stereological techniques. The approximation of microcracks by straight lines enables researchers to draw maps of the sample crack network over an area of a few tens of square centimeters. Various tests were carried out to verify the accuracy and the reproducibility of the results yielded by the method. Results obtained for undamaged and mechanically loaded samples are also presented.

Keywords: Durability; Microcracking; Image analysis; Mechanical loading

1. Introduction

Whatever its origin (mechanical, physical, or chemical), the degradation of cement-based materials often results in the initiation and the propagation of microcracks. Over the past decade, numerous studies have clearly indicated that the presence of microcracks can significantly influence the mechanical and mass transport properties of concrete [1–4]. The optimization and/or the prediction of the material macroscopic properties therefore require the development of a reliable tool that is capable of quantifying the material microstructural characteristics.

Over the past 20 years, several techniques have been developed to detect and measure microcracks in cement-based materials [5–14]. The advantages and drawbacks of each of these methods have been critically discussed in a previous paper [10]. The main difficulties with microcrack measurements in cement-based materials can be summarized as follows:

1. Most sample preparation techniques require a predrying treatment that can alter the original state of the material. The hydrated cement paste is a moisture-sensitive material in which even the slightest drying can induce microcracks.
2. Manual counting of microcracks is tedious and constitutes a limitation for a systematic analysis. Test results may also be biased by the subjectivity of the operator who often has to convert a complex picture into a binary (yes/no) result [12].
3. Microcrack measurements can significantly vary with the magnification used during the observations. Such a phenomenon originates from the heterogeneous and multiscale structure of cement-based materials [13].

More recently, Darwin et al. [14] proposed a new technique to detect and count microcracks in neat cement paste samples. According to this approach, the hydrated cement paste samples are polished, impregnated with a epoxy resin, and observed using a scanning electron microscope (SEM) in backscatter electron mode. Despite the good contrast obtained with this technique, the authors report that the reli-

* Corresponding author. Tel.: 418-656-2079; fax: 418-656-3355.
E-mail address: jmarchan@gci.ulaval.ca (J. Marchand)

0008-8846/00/$ – see front matter
PII: S0008-8846(99)00212-4

ability of the crack network characteristic determination is affected by variations in grey levels in the impregnated cracks. In backscatter imaging, the contrast between two phases depends on the ratio between their respective average atomic numbers; the grey levels in the crack area are directly influenced by the underlying and adjacent solid phases. The authors developed a new image-processing strategy to minimize the influence of this phenomenon on the detection procedure.

A new technique that allows the automatic detection and quantitative determination of microcracks in cement-based materials is presented in the following sections. The technique was developed to assess the characteristics of the crack network of mortar and concrete samples. In contrast to the procedure of Darwin et al. [14] that has been designed to investigate the material at the microscopic scale, this new technique operates at the mesoscopic scale. The technique is essentially a three-step process that includes the preparation of the sample, the automatic detection of microcracks, and the mathematical treatment of the collected data. During the development of the method, various tests were carried out to assess the reliability and reproducibility of the process. Results of these tests are presented along with a detailed description of the method.

2. Microcrack detection using an impregnation technique

A simple dye impregnation technique was developed to avoid any bias, which can be induced by the sample preparation. The procedure has been extensively described in a previous paper [10]. The method is briefly summarized in the following list:

1. A 15-mm thick disc of concrete is first cut and polished under water to obtain a smooth surface.
2. The wet polished surface is then impregnated with a red dye solution (or a fluorescent solution).
3. The excess dye is removed by polishing the sample with a 6-μm diamond paste.
4. Finally, progressive polishing with 3-and 1-μm diamond pastes guarantees a good surface quality.

The preparation technique is fast and relatively straightforward. Its main advantage lies in the fact that it does not induce any microcracks in the material [10]. Except for a very short period of air drying, during which the red dye penetrates the material pore structure, all other steps are carried out under water. It must be emphasized that the polishing operations that follow the impregnation are of primary importance. To obtain accurate results, the red dye must be retained only in microcracks and voids as shown in Fig. 1A.

Previous experience has shown that observations of the polished surface (using an optical microscope at a magnification in the range of 10 to 300×) is sufficient to highlight the material defects and to allow the detection of microcracks, paste-aggregate transition zones, porous areas, and air bubbles. When applied to ordinary concrete, the technique generates images with a good contrast, which are convenient for quantitative analysis.

Experience has also shown that the contrast is, however, weaker when denser matrices (mixtures of low water/binder ratios or containing mineral additions like fly ash or silica fume) are tested. Furthermore, dense systems are difficult to impregnate. In this case, a fluorescent agent replaces the red dye. Fluorescent dye impregnation techniques have been extensively used for years in other fields such as biology [15]. Recent work by Gran [16] has clearly shown that these

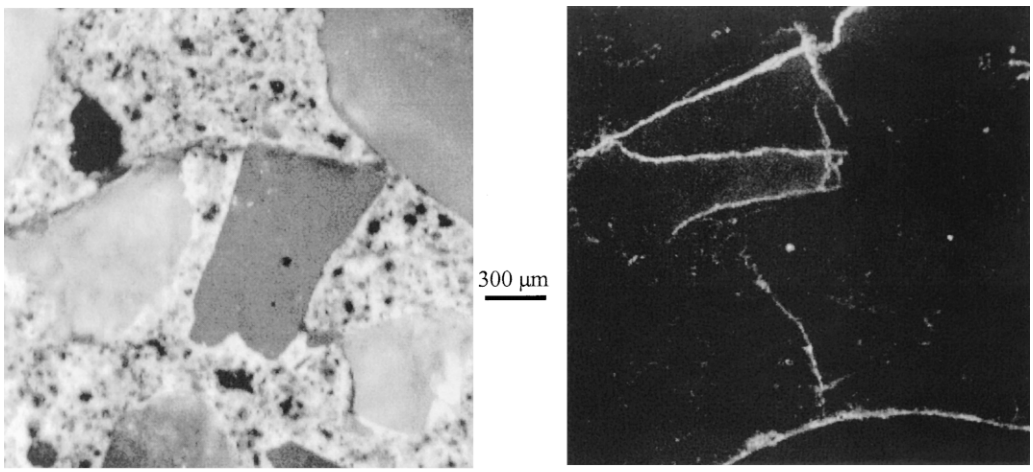

Fig. 1. Microcracks in impregnated samples (magnification 40×). (A) Sample impregnated with a red dye. (B) Sample impregnated with a fluorescent solution.

techniques are well suited for microcrack observation in high-performance concrete.

The preparation steps for the fluorescent dye impregnation are similar to those used for the red dye impregnation technique. The only difference is that the concrete sample has to be immersed for four days in a fluorescent solution of ethanol. During this time, the fluorescent alcohol, which also penetrates within microcracks and voids, progressively replaces the concrete pore solution. After the immersion period, the sample is polished under water. The sample is then ready to be observed using an optical microscope under ultraviolet light (see Fig. 1B).

3. The image analysis procedure

The various aspects of the automatic detection of the microcracks and the mathematical treatment of the collected data are described in the following paragraphs. Special attention is given to the mathematical algorithms developed to analyze the collected data.

3.1. Equipment

All algorithms for the image analysis operations were developed using the VISILOG 4 software (Noesis S.A., Orsay, France). The image acquisition from the optical microscope is made using a tri-CCD color camera (Noesis, S.A.) that is linked to a personal computer. Images are digitized using a Matrox image 640 card (Noesis, S.A.). The automatic field by field displacements of the sample is controlled by a motorized stage x-y-z controlled from the microcomputer.

3.2. Microcrack identification algorithm (segmentation)

The procedure first involves the acquisition of a 256 × 256-pixel color image (Fig. 2A). Three different black and white images are then derived from the original color image on the basis of its R (red), G (green), and B (blue) components. Each of these three images contains 256 possible grey levels ranging from 0 for black to 255 for white. If the sample has been impregnated with a red dye, the following arithmetical operation is performed to highlight the impregnated microdefects [see Eq. (1)]:

$$O(x, y) = \max\begin{cases} R(x, y) - G(x, y) \\ 0 \end{cases} \quad (1)$$

In Eq. (1), $O(x, y)$ stands for the intensity of the pixel of coordinates (x, y) in the output grey level image. $R(x, y)$ and $G(x, y)$ are the intensities of the same pixel in the red and green images, respectively. In the image thus obtained (Fig. 2B), the pixels corresponding to defects are notably clearer than the background (Fig. 2C). This operation aims at facilitating the next stage of thresholding. If the material has been impregnated with a fluorescent dye, the contrast of the green component is sufficient, and all the following operations are carried out on this image only.

To assess the characteristics of the crack network, it is necessary to convert the image (that may contain up to 256 possible grey levels) into a binary image. In this binary image, the pixels defining the defects are assigned a value of 1 and the background pixels are given a value of 0. The thresholding is probably the most critical operation. In general, the larger the contrast in intensity between the objects and the background, the easier the thresholding operation. The thresholding operation may be carried out manually or automatically. In the manual (interactive) procedure, the operator himself defines the appropriate boundary values. The determination of the proper values can be done on the basis of previous tests. In that respect, automatic thresholding methods present numerous advantages over the manual procedure. For instance, they can easily account for any variation in the contrast between two successive images originating from the same sample (or originating from two samples of the same mixture) [17]. These variations are generally related to the heterogeneous nature of the material. They can also be induced by the sample preparation operations.

During the development of this method, various statistical thresholding methods (based on the histogram of grey levels) were evaluated and compared. The entropy maximization method [18] was found to yield the best results. It was found that the threshold values obtained on the basis of this method were consistently similar to those obtained manually by an iterative process.

The entropy maximization method consists in determining, for a given image O, the grey levels, (s), that maximize the entropy function $\Phi(k)$. The entropy function is computed according to Eq. (2):

$$\Phi(k) = -\left[\sum_{\min}^{k}\left(\frac{p_i}{w_0}\right)\cdot\log\left(\frac{p_i}{w_0}\right) + \sum_{k+1}^{\max}\left(\frac{p_i}{w_1}\right)\cdot\log\left(\frac{p_i}{w_1}\right)\right] \quad (2)$$

Where p_i is the probability for a given pixel to have an intensity equal to i ($p_i = N_i/N$), Ni is the number of pixels that have the i intensity, and N is the total number of pixels. w_0 and w_1 are, respectively, the probability to found a pixel intensity lower or higher than

$$(k)\left(w_0 = \sum_{\min}^{k} p_i;\ \ w_1 = \sum_{\mathrm{kH}}^{\max} p_i\right).$$

Once the (s) value is computed, the lower bound thresholding is then operated according to Eq. (3):

$$B(x, y) = \begin{cases} 0 & \text{if} \quad O(x, y) < s \\ 1 & \text{if} \quad O(x, y) > s \end{cases} \quad (3)$$

Following the thresholding operation, the resulting binary image (B) is then transformed by two successive morphological operations of eroding and rebuilding. These operations eliminate noise and small objects (<10 pixels) for which the measurements are not well adapted. Fig. 2D illustrates the image obtained after these treatments.

The initial treatments of the image based on the charac-

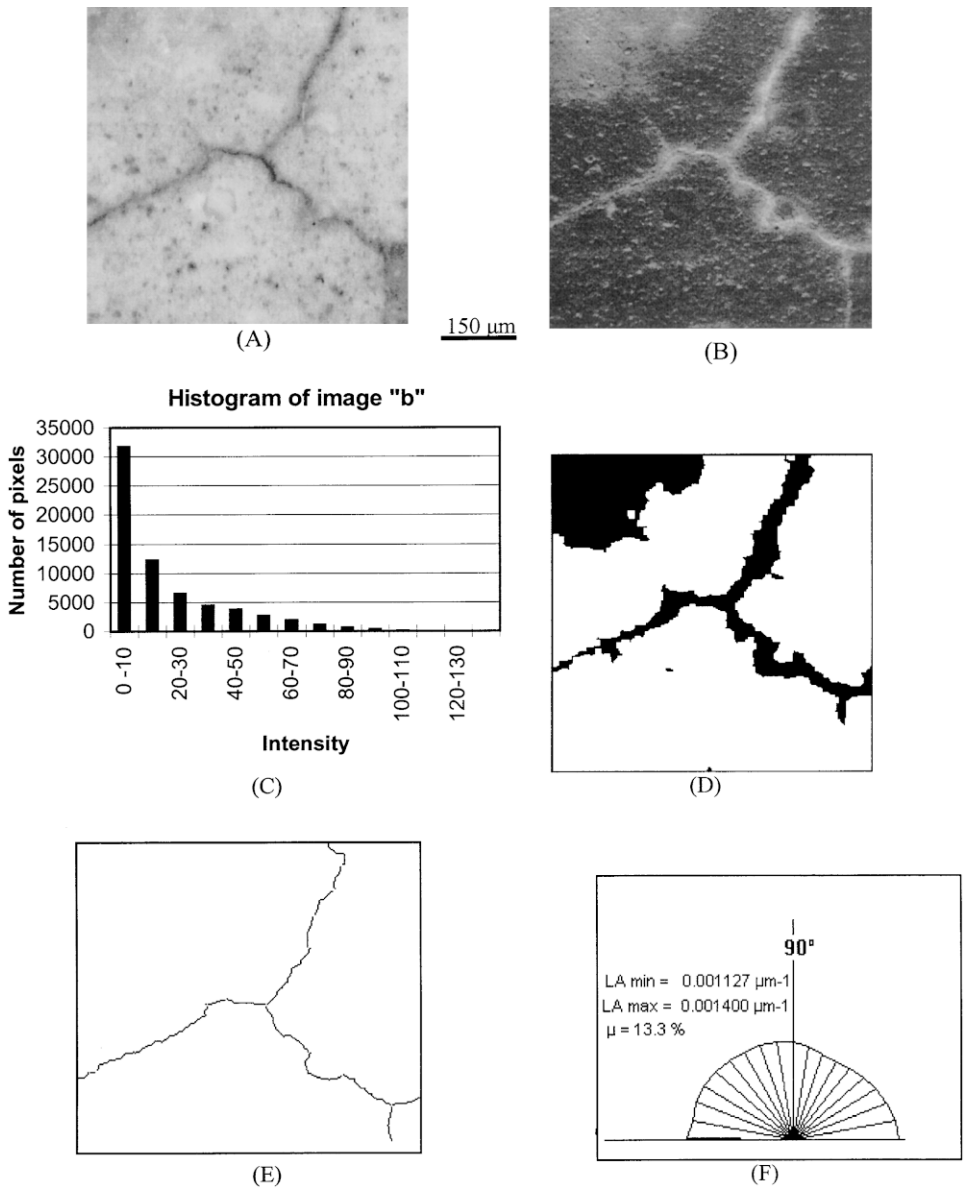

Fig. 2. (A) Original color image; (B) grey level-enhanced image; (C) histogram of image B; (D) binary image after thresholding; (E) treated microcrack network; and (F) rose of specific crack length.

teristic grey level of impregnated defects are not sufficient to distinguish cracks from other defects. A second series of operations, during which shape criteria are used, is therefore necessary. Cracks can sometimes be individual objects with an elongated shape, but more frequently they are arranged into a connected network. Several size criteria and various shape factors have been tested [19].

Initially, a criterion of minimal elongation [see Eq. (4)]:

$$F_E > 1.5 \tag{4}$$

where F_E is length-to-width ratio, has allowed reliably identification of individual cracks. However, branching cracks are not as easy to deal with. A significant part of these cracks has low F_E values, close to that of pores and voids. The sole utilization of criterion [4] was found to be insufficient. The use of a circularity factor (ρ = perimeter$^2/4\pi$ area) did not yield good results, very probably because the perimeter estimate is very sensitive to small errors in the contour value [19–21]. The criterion, which was found to be the most appropriate to discriminate between cracks and other defects (porous zone, voids, etc.), is a dimensionless packing density index F_c given by Eq. (5):

$$F_c = \frac{A_{ob}}{A_{cc}} \tag{5}$$

Where A_{ob} is the object area and A_{cc} is the area of its circumscribed circle for which the diameter is the maximum value of Ferret's diameter [19] computed at every 10 degrees. F_c

is equal to 1 for a circle and tends toward 0 for a very elongated object, typically an individual crack. Furthermore, F_c is smaller for a concave object (e.g., a branching crack) than for a rather compact object (porous zone or void).

An automatic ranking of cracks requires the determination of a threshold value F_{cs} that can be used to separate cracks with a good degree of reliability. For this purpose, a statistical analysis of F_c values for various crack networks was realized. Fig. 3 gives the cumulative probability of F_c for a composite set of cracks that contains cracks of various shapes. As can be seen, all cracks have a factor lower than 0.24, and for 94% of them it does not exceed 0.20. Furthermore, it was observed that values ranging between 0.20 and 0.24 often correspond to limit cases like, for instance, porous zones connected to cracks. On the basis of this analysis, the value F_{cs} was fixed to 0.20 [see Eq. (6)]:

$$F_C < 0.2 \tag{6}$$

The validity of this criterion has been verified for the range of magnification (25 to 80×) used in this study. Fig. 4 shows three different types of cracks and a porous zone and the computed values of F_E and F_c.

Once microcracks are been sorted out of the other objects, it is possible to store them in a new image. The next step of the treatment consists of reducing the objects to their skeleton (i.e., to curves of unit width). During the skeletonization step, the algorithm must recognize and remove "dead ends" that can appear due to irregularities in the contour of the objects. Only dead ends whose lengths are larger than 10 pixels are kept during the treatment (Fig. 2E). Finally, a routine identifies the extreme points of each composite crack. These points are located within a given (fixed) system of coordinates (accounting for the displacements of the specimen from one field to another) and they are stored.

3.3. Quantification of microcracks

The basic characteristics of the microcrack pattern are determined on the basis of classical stereological methods. During the development of this image analysis procedure, two different stereological techniques [22] were tested: (1) the method of the oriented secants on a plane, and (2) the method of total projections.

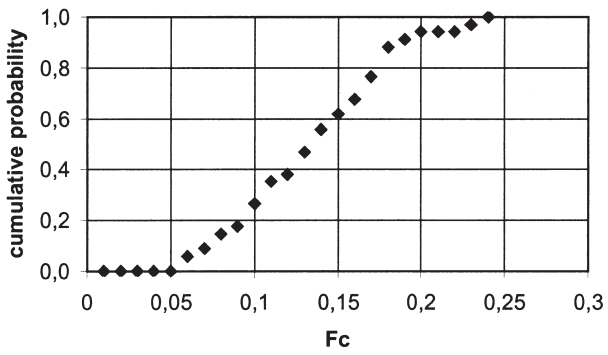

Fig. 3. Distribution of F_c values for microcracks.

The oriented-secant method consists of covering the treated image with an ensemble of parallel equidistant lines. The system is characterized by the spacing between two lines and their angle with a reference system of coordinates. Using an automatic procedure implying logical binary operations of the images, the number (N_L) of common points between the cracks and the set of lines is computed for several orientations from 0 to 180° by 10° steps. A polar representation of N_L is then drawn, which shows the degree of orientation of the microcrack pattern. The local degree of the orientation of the microcrack pattern is finally computed according to Eq. (7):

$$\omega = \frac{(N_{L\,\max} - N_{L\,\min})}{N_{L\,\max} + \left(\frac{\pi}{2} - 1\right) \cdot N_{L\,\min}} \qquad (0 \leqslant \omega \leqslant 1) \tag{7}$$

Where $N_{L\max}$ and $N_{L\min}$ are the maximum and minimum values taken by N_L (θ) when θ varies. ω takes the value 0 for a perfectly isotropic cracking pattern (i.e., with no special orientation) and the value 1 when all the microcracks have the same orientation. The total projection rule stipulates that the specific number of intersection N_L (θ) between the system of lines and the microcracks network corresponds to the specific projected $L_{A\text{proj}}$ in a direction orthogonal to θ (Eq. 8):

$$N_L(\theta) = L_A\left(\theta + \frac{\pi}{2}\right) = L_{A\,\text{proj}} \tag{8}$$

In the case of isotropic cracks, there is an important relationship between the average number of intersections N_L (which is in this case independent on θ), the total specific length and the specific area of cracks S_V (mm^2/mm^3) [see Eq. (9)]:

$$\frac{\pi}{2} \cdot N_L = L_A = \frac{\pi}{4} \cdot S_V \tag{9}$$

Microcracks can also been quantified by using the total projection method. In this case, one uses the Ferret's diameter to quantify the projected length of microcracks per unit area or the specific crack length L_A(θ) for various orientations θ (in mm/mm^2). A polar representation of L_A (θ) (rose of specific crack length) is given at Fig. 2F. The degree of orientation can be computed using Eq. (10):

$$\omega = \frac{L_{A\text{or}}}{L_{A\text{tot}}} = \frac{L_{A\text{or}}}{L_{A\text{or}} + L_{A\text{iso}}} \qquad (0 \leqslant \omega \leqslant 1) \tag{10}$$

Where $L_{A\text{iso}}$ and $L_{A\text{or}}$ are, respectively, the isotropic and oriented specific lengths and where $L_{A\text{tot}}$ is the total specific length of cracks. As can be seen, Eq. (7) can be obtained from Eq. (10) by introducing the rule of total projections Eq. (8) and Eq. (9).

Experience has shown that both methods yield globally the same results. Such an observation is in good agreement with what is usually reported in the literature [23]. However, the method of total projections is less time-consuming (by a factor approximately 3). In the following applications,

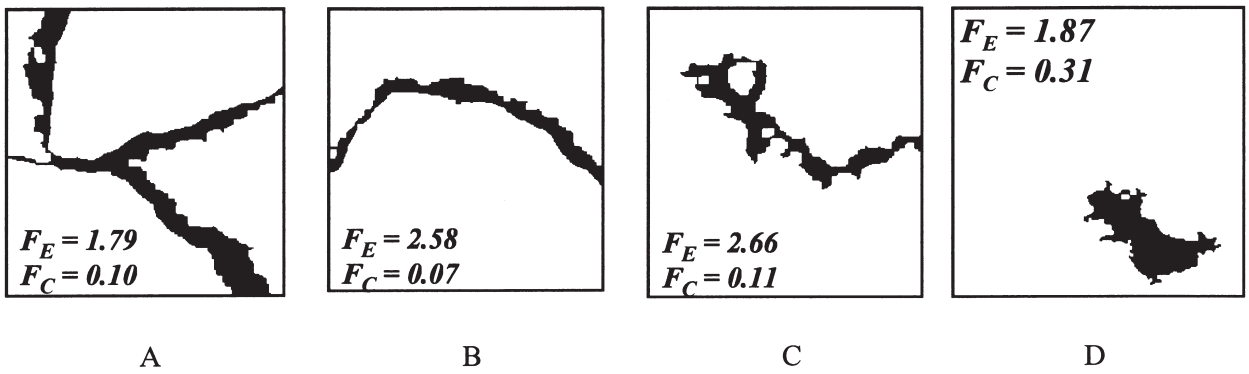

Fig. 4. Shape factors (F_E and F_c) for various types of defects: (A–C) cracks; (D) porous zone.

all the characteristics of the various microcrack patterns that will be presented have been calculated using the method of the total projections.

3.4. Reconnecting fields

Large cracks are known to have a major influence on macroscopic properties like permeability or Young's modulus. However, their weight on measurements such as N_L or L_A is only negligible. The algorithm therefore must be able to identify and quantify macrocracks properly. The main difficulty of this operation arises from the fact that cracks can extend on several neighboring microfields. If no particular attention is paid to this particularity, large cracks will be counted as several different smaller cracks with no error on N_L or L_A measurements, but with a significant error on the prediction of the material physical properties that will be drawn from crack pattern estimates.

As part of the development of our image analysis procedure, a specific algorithm has been developed to reconnect large cracks and thus avoid biases due to these problems [24]. The problem is simplified by considering only the crack ends stored in each field. For each crack (i) contained in a given field, all potential "twin" cracks (j) in the neighboring fields are tested. Two criteria must be fulfilled for connecting i and j cracks:

1. The distance between two cracks must be lower than Δ_{max}, which is an error value due to the imperfect translation of the specimen (mechanical gap in the guidance system of the stage) and which has been carefully estimated.
2. The angle between the two cracks must be larger than 90 °.

A simplified description of the image analysis procedure is given in Fig. 5.

4. Validation of the method

During the development of this technique, several tests were performed to validate the various steps and algorithms of the image analysis procedure. Some of these tests were carried out on real cracked materials, while others dealt with model (artificial) specimens.

To validate the portion of the algorithm that had been developed to reconnect the various fields together, we have analyzed a bundle of 24 metallic fibers (approximate length 12 mm, diameter 0.1 mm) at a magnification of 20×. At this magnification, the elementary field size is 3.6 mm and the macroscopic image contains 416 elementary fields. Fig. 6A shows the first result of the analysis, where the object size is limited by the field size. Fig. 6B gives the size distribution after reconnecting. As can be seen, the large majority (23 of 24) of the objects are in the 11- to 14-mm interval, which validates the algorithm.

4.1. Sources of error

The electronic treatment can induce noise in the image. This noise can subsequently modify the shape of the objects after thresholding and therefore the microcrack density. This effect can be quantified when the entire process is performed twice while all parameters are kept constant. By summing images obtained through successive acquisitions, it is possible to make the noise spatially uniform, therefore improving the signal/noise ratio [17]. Trial tests indicate that summing six images (of the same field) gives a coefficient of variation of the microcrack length of about 10%. Each initial image is thus built by repeating the acquiring phase six times.

Another source of error comes from the threshold value of the shape factor F_c, set at 0.2 [see Eq. (6)]. In the case of highly microporous cement pastes in which cracks are linked to pores or cannot even be distinguished from the porosity, this value is questionable. However, as soon as the material has a sufficient density, the threshold value yields correct results. It is important to note that a preparation of quality (uniformity of impregnation and polishing) is an essential demand of the technique at all stages of the processing.

4.2. Reproducibility and magnification effect

A test was performed to verify the reproducibility of the measurement and the influence of the magnification factor. A 0.38 water/cement ratio concrete was subjected to a heat

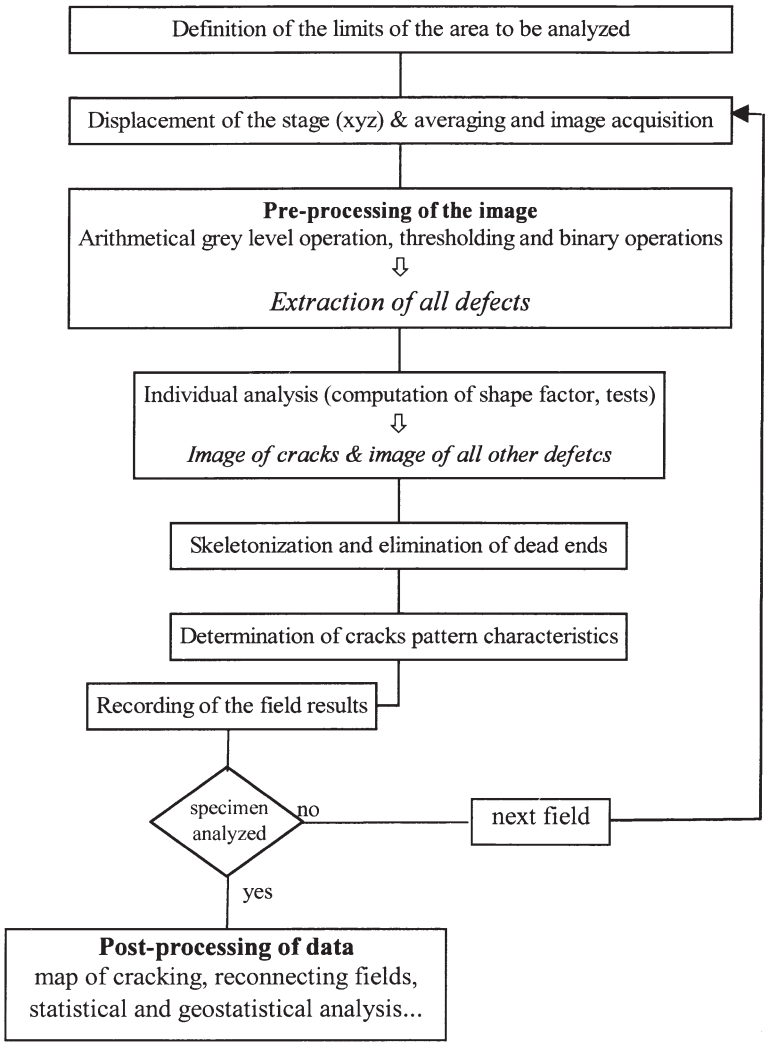

Fig. 5. Description of the image analysis procedure.

curing treatment at 50°C during 8 h, then kept at 20°C in the laboratory. After preparation, a surface of 3.5 cm^2 of concrete has been analyzed three times for each of the three following magnifications factors: 25, 40, and 80×. As can be seen from Fig. 7, good reproducibility is obtained for the three tests carried out at the same magnification. Specific crack length values and degrees of orientation are similar for all measurements. The measured degrees of orientation (which range from 4 to 6.3%) are characteristic of a weakly oriented pattern. The results also indicate that the crack length is very sensitive to the magnification factor, since it is doubled with magnifications from 25 to 80×. A higher magnification allows detection of smaller defects. However, the degree of orientation appears to be affected much less by a change on the magnification.

5. Study of materials subjected to a mechanical loading

The image analysis technique has been applied to two mechanically damaged cement-based materials. The first one is a high-performance concrete that had been loaded in uniaxial tension. The second one is a mortar subjected to uniaxial compression. Table 1 gives all information on the mixtures and their respective mechanical properties.

5.1. High-performance concrete in tension

Samples of high-performance concrete were tested in uniaxial tension according to the BIPEDE procedure [3,25–28]. Test specimens had a diameter of 110 mm and a thickness of 40 mm. To produce samples with different cracking patterns, three levels of loading were selected. A first series of specimens were tested, up to a maximum strain of 2×10^{-4}, a second series was brought to a maximum strain of 6.5×10^{-4}, and a third series was tested to a maximum strain of 8×10^{-4}.

At the end of the mechanical test, the concrete specimens were impregnated with a fluorescent solution. A rectangular area of 41 cm^2 in the central part of the disc was analyzed at a magnification factor of 40×. Table 2 gives the specific

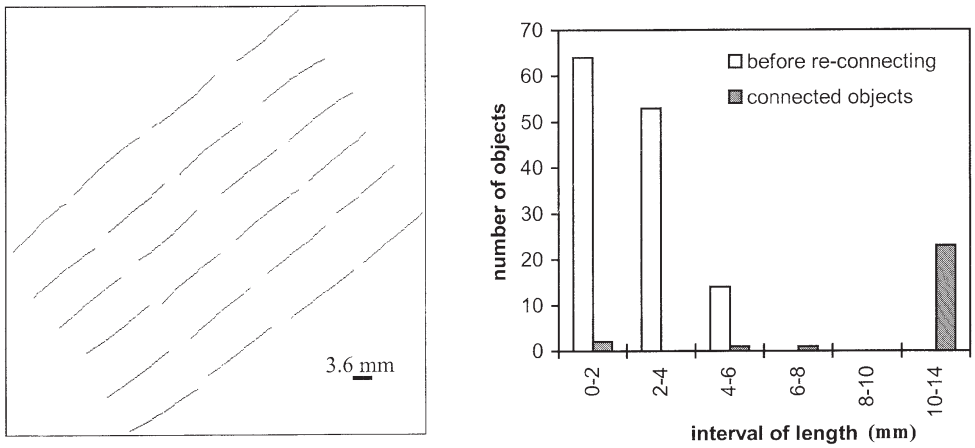

Fig. 6. Evaluation of the reliability of the reconnecting algorithm.

crack length, degree of orientation, and percentage of the uncracked area within specimen.

As can be seen in Table 2, an increase in loading from *A* to *B* significantly increases the specific length as well as the degree of orientation. However, no significant change in the values of those two parameters is observed when loading is further increased from *B* to *C*. Closer examination of the cracking patterns (Fig. 8) provides additional information. These patterns show the coexistence of two localized cracks at the levels *B* and *C*, which are more or less continuous throughout the specimen. These cracks are perpendicular to the axis of loading and do not exist at the initial level of loading (level *A*). The presence of these macrocracks contributes highly to the degree of orientation of the crack network. The measurements confirm that the cracking pattern is not significantly modified once it has been created. At this stage, all global deformations of the specimen correspond to the gradual opening of the existing macrocracks. Unfortunately, the mean value of the crack opening can hardly be calculated on the basis of the image analysis procedure.

A complementary study of the third specimen (level *C*) consisted in using two different magnification factors for an investigated area of 8 × 2.7 cm. Magnifications of 40 and 20× have been used (respectively, corresponding to a pixel size of 7.2 and 14.4 μm and to a number of 640 and 160 elementary fields). While the crack specific length is only slightly affected by the magnification (7.5×10^{-2} mm^{-1} at 20×, 8.7×10^{-2} mm^{-1} at 40×, which corresponds to an increase of approximately 16%), the degree of orientation is decreased by 30% (36.8% for 20× and 27.7% for 40×). These results confirm that a lower magnification is more sensitive to the anisotropy. A higher magnification reveals more defects, which are more isotropic, and this lowers the degree of orientation.

5.2. Mortar under uniaxial compressive loading

The cracking pattern of a second series of samples that had been subjected to mechanical compressive loading was also determined. The measurements were carried on a series

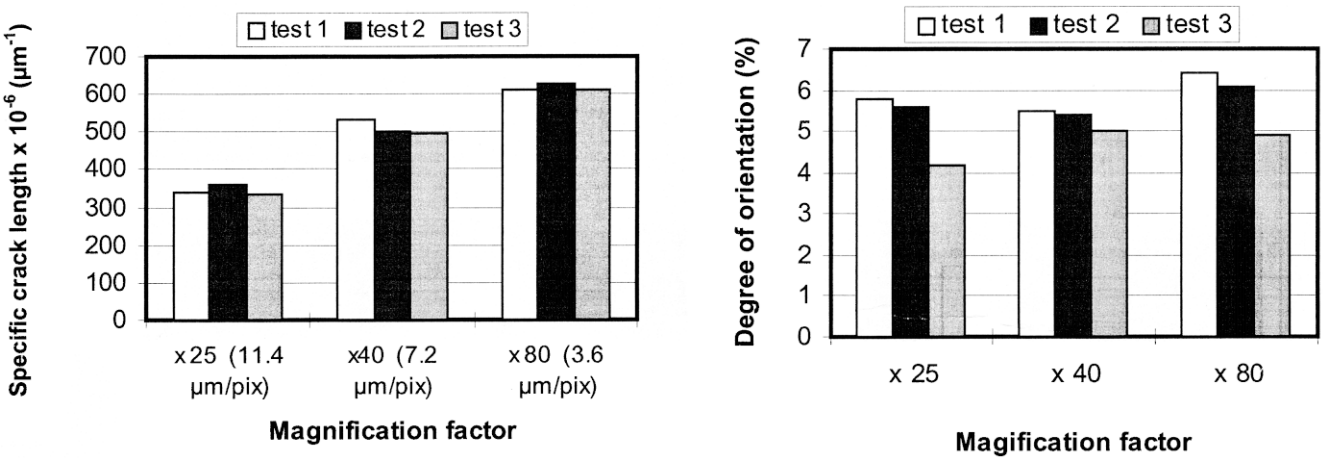

Fig. 7. Reproducibility of the test results and influence of the magnification.

Table 1
Mixture characteristics and mechanical properties of the materials

Constituents	High-performance concrete	Mortar
Cement ordinary Portland cement	400 kg/m^3	639 kg/m^3
Silica fume	40 kg/m^3	–
Water	120 kg/m^3	256 kg/m^3
Fine sand	746	966 kg/m^3
Coarse sand	–	414 kg/m^3
Gravel 4–10 mm	1,145	–
Superplasticizers	yes	no
Slump	200 mm	–
Water/binder	0.3	0.4
E average	45,000 MPa	–
f_c average	91.3 MPa[a]	69 MPa[b]
f_t average	6.5 Mpa[a]	–

[a]at 28 days; [b]at 42 days.

Table 2
Crack pattern characteristics of the high-performance concrete tested in tension

Level of loading	Strain $\times 10^{-4}$	Specific crack length $L_{Atot} \times 10^{-2}$ (mm/mm^2)	Degree of orientation ω (%)	(Virgin/total) area (%)
A	2.0	1.30	8.50	92
B	6.5	8.06	16.0	81
C	8.0	8.11	17.6	67

of mortar samples. The analysis was performed on a first series of three reference samples (named T_1, T_2, T_3) that were not subjected to any loading. The three reference samples were sawn from the central part of three cylinders (110 mm diameter, 220 mm length). A second series of three samples (named P_1, P_2, P_3) was also analyzed. These samples were sawn off a cylinder that had been loaded at its ultimate strength (peak load). Discs P_1, P_2, and P_3 were taken at three different locations within the cylinder (distances of 20, 30, and 100 mm from its end).

Table 3
Crack pattern characteristics of a mortar subjected to a compressive loading

Specimen	Specific crack length $L_{Atot} \times 10^{-2}$ (mm/mm^2)	Degree of orientation ω (%)	(Virgin/total) area (%)
T1	25	7.3	17
T2	28	9.4	33
T3	16	13.5	57
Average	23	10.1	35.7
Coefficient of variation (%)	27.1	31.2	56.4
P1	38	7.7	16
P2	43	6.7	16
P3	37	8.5	9
Average	39.3	7.6	13.7
Coefficient of variation (%)	8	11.8	29.5

After the impregnation with the red dye, an area of 11.6 cm^2 in each disk was analyzed at a magnification of 40×. The crack pattern characteristics of each sample are summarized on Table 3.

Test results indicate a significant difference for the microcrack specific length between the reference and the loaded samples (with an average increase of 71%). Furthermore, the previous mechanical loading appears to reduce the scatter on L_{Atot} between the samples. The same can be said about the variability of undamaged area.

For the loaded sample, the microcrack specific length does not appear to vary markedly along the axis of the cylinder. It is also clear that in the plane of analysis (perpendicular to the axis of loading), the degree of orientation is low

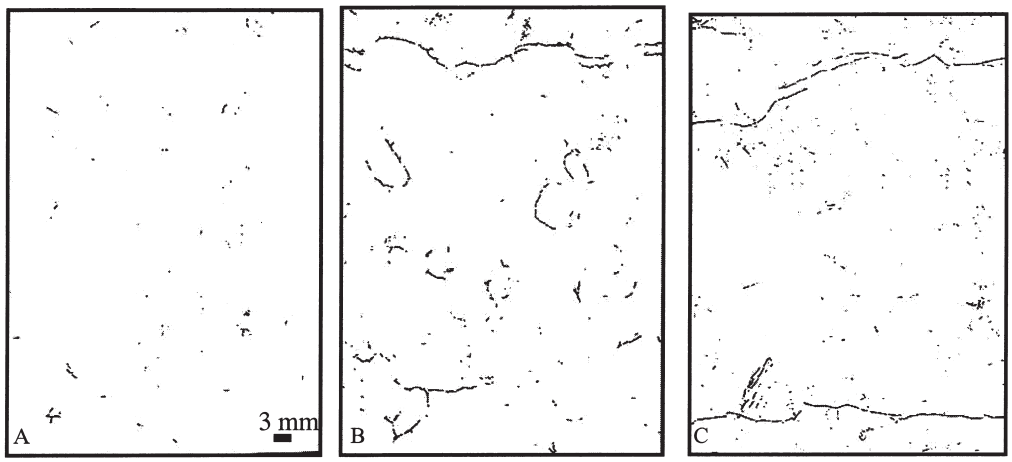

Fig. 8. Crack patterns for three levels of loading: (A) $\epsilon_{max} = 2 \times 10^{-4}$; (B) $\epsilon_{max} = 6.5 \times 10^{-4}$; (C) $\epsilon_{max} = 8.0 \times 10^{-4}$.

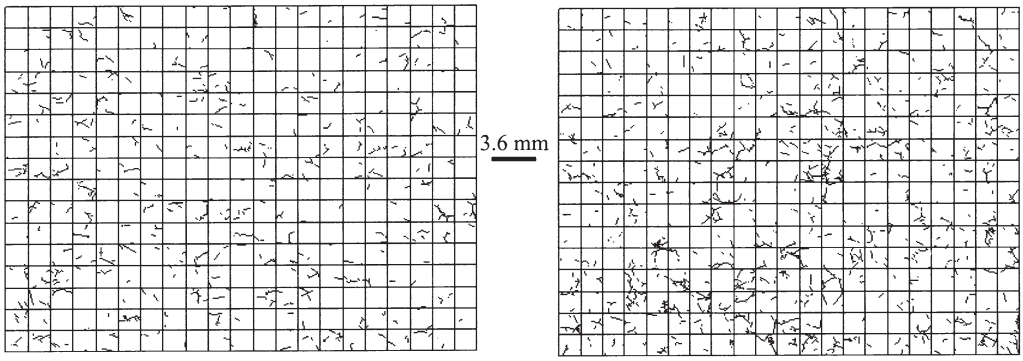

Fig. 9. Crack patterns of the mortar samples: (A) virgin and (B) loaded at peak stress.

and remains unaffected by loading. Fig. 9 confirms that the cracking pattern appears spatially homogenous within the specimen at this scale.

6. Concluding remarks

A technique for the quantification of microcracks in cement-based materials has been developed. It includes:

- an experimental process during which samples are impregnated without inducing any spurious microcracking;
- algorithms for the image analysis that enable determination of the crack pattern characteristics (i.e., the specific crack length and the degree of orientation) of a given sample and to map the defects.

Various tests run as part of the development of the method have shown that the image analysis algorithms are reliable and lead to reproducible results. The whole process makes possible the systematic analysis of specimens of a significant size (with respect to the mechanical representative elementary volume of the material) that have been damaged by various mechanisms. The measurements can be qualitatively as well as quantitatively compared for several magnifications.

Among the first results, the crack pattern of high-performance concrete samples that had been subjected to tensile loading was determined. The sensitivity of the two crack pattern parameters to the magnification factor has been evaluated on the basis of these results. This point will be further studied in the future and results will be used in the framework of micro-macro mechanical models.

Future research will also focus on the identification of the relevant scale at which the material can be considered as statistically homogeneous (representative volume element). This evaluation will be made on the basis of micromechanical considerations.

Acknowledgments

The authors are grateful to Electricité de France (EDF/DER) for its financial support for the project and the Laboratory Network GEO for cooperation around this topic. The authors would also like to thank J. Riss for her scientific and technical help.

References

[1] D. Ziegeldorf, Phenomenological aspects of the fracture of concrete, in: F.H. Wittman (Ed.), Fracture Mechanics of Concrete, Elsevier Science Publishers, Amsterdam, 1983, p. 31.
[2] E.K. Attiogbe, D. Darwin, Submicrocracking in cement paste and mortar, ACI Mat J 84 (1987) 491–500.
[3] B. Gérard, D. Breysse, A. Ammouche, O. Houdusse, O. Didry, Cracking and permeability of concrete under tension, Mater Struct 29 (1996) 141–151.
[4] H.R. Samaha, K.C. Hover, Influence of microcracking on the mass transport properties of concrete, ACI Mat J 89 (1992) 416–424.
[5] F.O. Slate, S. Olsefski, X-rays for study of internal structure and microcracking of concrete, J Amer Conc Inst 60 (1963) 575–587.
[6] W.S. Najjar, H.C. Aderhold, K.C. Hover, The application of neutron radiography to study of microcracking in concrete, Cem Concr Agg 8 (1986) 103–109.
[7] F.O. Slate, in: F.H. Wittman (Ed.), Fracture Mechanics of Concrete, Elsevier Science Publishers, Amsterdam, 1983, p. 75.
[8] J.P. Ollivier, A nondestructive procedure to observe the microcracks of concrete by scanning electron microscopy, Cem Concr Res 15 (1985) 1055–1060.
[9] E. Ringot, E. Thèse de doctorat INSA de Toulouse, Université Paul Sabatier, 1988.
[10] H. Hornain, J. Marchand, A. Ammouche, J.P. Commène, M. Moranville, Microscopic observation of cracks in concrete—A new sample preparation technique using dye impregnation, Cem Concr Res 26 (1996) 573–583.
[11] H. Hornain, M. Moranville-Regourd, 8th International Congress on the Chemistry of Cement, Rio de Janeiro, Vol. 53, 1986.
[12] D. Darwin, K.W. Ketcham, F.A. Romero, J.L. Martin, Automated identification of compression-induced cracking in cement paste, Proc., ASCE Eng. Mech. Conf., College Station, Texas, 1992, pp. 494–497.
[13] M. Moranville-Regourd, La durabilité des structures en béton, Conf., ENPC, Paris, 1990.
[14] D. Darwin, M.N. Abou-Zeid, K.W. Ketcham, Automated crack identification for cement paste, Cem Concr Res 25 (1995) 605–616.

[15] A.M. Glauert, Practical Methods in Electron Microscopy, North-Holland/American, Elsevier, 1975.
[16] H. Chr. Gran, Fluorescent liquid replacement technique. A mean of crack detection and water-binder ratio determination in high strength concrete, Cem Concr Res 25 (1995) 1063–1074.
[17] J.C. Russ, Computer Assisted Microscopy, Plenum Press, New York, 1990.
[18] R. Zeboudj, Thèse de doctorat de l'Université de St-Etienne, France, 1988.
[19] M. Coster, J.L. Chermant, Précis d'analyse d'images, Presses du CNRS, Paris, France, 1985.
[20] J. Serra, Image Analysis and Mathematical Morphology, Academic Press, New York, 1981.
[21] S.A. Saltykov, A stereological method for measuring the specific surface area of metallic powders, in: H. Elias (Ed.), Proc. Second Int. Cong. for Stereology, Springer-Verlag, New York, 1967, p. 63.
[22] P. Stroeven, Ph.D. Thesis, University of Delft, 1973.
[23] E. Ringot, Automatic quantification of microcracks by stereological method of total projections in mortar and concrete, Cem Concr Res 18 (1988) 35–43.
[24] A. Ammouche, H. Hornain, Caractérisation de matériaux vieillis et fissurés par analyse d'images, Internal report LERM for EDF/DER, 1996.
[25] D. Breysse, B. Gérard, M. Lasne, Cracking and accelerated deterioration of concrete, Third CANMET/ACI Int. Conf. on Durability of Concrete, Nice, France, 1994.
[26] A. Ammouche, DEA MAISE, LMT Cachan, France, 1993.
[27] B. Gérard, Ph.D. thesis, Laval University, Québec, ENS Cachan, France, 1996.
[28] B. Gérard, J. Marchand, D. Breysse, A. Ammouche, Constitutive law of high-performance concrete under tensile strain, 4th International Symposium on utilization of high-strength concrete, BHP 96, Paris, Vol. 2, 1996, pp. 677–685.